

Experimental and Numerical Investigation on Aerodynamic Performance of a Mars Rotor System

Yi Liu¹, Jun Xiao¹, Ndouba Ange Benai-dara¹, Zhaolin Chen¹ & Ning Qin²

¹State Key Laboratory of Mechanics and Control of Mechanical Structures, NUAA, Nanjing, Jiangsu, China ²Professor of Aerodynamics, Department of Mechanical Engineering, University of Sheffield, Mappin Street, Sheffield, S1 3JD, UK

Abstract

This study shows the aerodynamic performance and flow characteristics of the optimized Mars rotor (single-rotor and contra-rotor systems) through experimental and numerical simulation methods. Given the unique flight environment of Mars characterized by low Reynolds numbers and high Mach numbers, traditional rotor designs are inadequate to meet the demands of Martian flight. Therefore, this study designed three sets of rotors based on the optimized two-dimensional airfoil profiles, and conducted experimental and numerical simulation research under simulated low-pressure and -density conditions. Initially, we conducted experiments and numerical validations using standard APC propellers to assess the accuracy of the experimental force measurement system constructed in this study. The experimental error is within 5 %, which proves that the accuracy meets the experimental requirements. Secondly, experimental data of machined rotors were obtained under low-pressure and -density conditions and compared with numerical simulations. The rotors were ultimately customized to suit the Martian environment, and numerical computations were utilized to investigate the influence of different tip Mach numbers on the hovering performance. It is shown that the rotor designed in this paper has good aerodynamic performance in Mars environment, which also provides ideas and methods for further improvement and research.

Keywords: Mars rotor design, Low reynolds number aerodynamic, airfoil design, rotor aerodynamic performance

1. Introduction

Rotorcraft enhance the potential for exploration by extending the range and velocity achievable in traversing targeted Martian sites of scientific interest. This capability unlocks mission possibilities that were previously deemed unfeasible, such as conducting scientific investigations in regions characterized by high elevations, rugged terrains, caves/lava tubes, and comprehensive surveys of the lower atmosphere. The contra-rotor system, an innovative approach entailing two rotors rotating in opposite directions along a shared axis, presents a potential solution to some of the challenges posed by Martian aeronautics. However, Mars' atmospheric density is merely 1% that of Earth's while possessing low surface sound speed[1]. Its distinctive compressible low Reynolds number and high Mach number flight environment restricts the suitability of airfoils available for use, thereby emerging as a significant predicament in Mars aircraft rotor design.

Due to the influence of the solar cycle, the atmospheric temperature on the surface of Mars varies in accordance with density. In 2020, J Pla-García et al. utilized a nested simulation method combining the Mars Regional Atmosphere Modeling System (MRAMS) and the Mars Weather Research and Forecasting Model (MarsWRF)[2] to predict local meteorological conditions in Jezeiro crater, which serves as the landing site for the Mars 2020 Perseverance rover. Figure 1 illustrates seasonal fluctuations in simulated diurnal pressure and surface temperature signals within this region. It is evident that at a sun longitude (Ls) of 180°, atmospheric temperature reaches 285 K while pressure stands at 640 Pa; however, it should be noted that atmospheric density merely amounts to 0.012, potentially exceeding operational limits for unmanned aerial vehicles on Mars.

INSERT RUNNING TITLE HERE

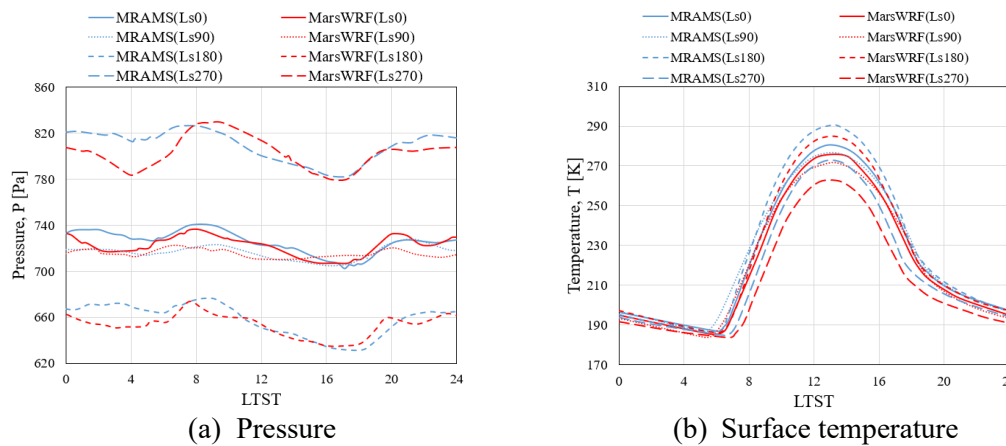


Figure 1 Modeled diurnal pressure and surface temperature signals for Jezero crater using MRAMS (blue curve) and MarsWRF (red curve), from Pla-García J et al.[2]

The Reynolds number is defined as the ratio of inertial force to viscous force in a fluid. In the low Reynolds number range, starting below approximately $Re_c \approx 10^5$, the dominance of viscous forces leads to a pronoused limitation on the maximum lift-drag ratio[3]. The occurrence of complete laminar flow at chord Reynolds numbers below 30,000 is possible for small angles of attack. As the incidence increases, adverse gradients become more severe and result in laminar separation, which limits the lift coefficient and significantly enhances drag. The low Reynolds number-transonic condition, however, exhibits a stretched trailing-edge separation pattern, indicating the suppression of compressible flow on the early separated shear layer roll-up motion and thereby preventing vortex shedding[4, 5]. The researchers conducted a detailed study on the inherent aerodynamic characteristics, separation phenomena, and other performance features of low Reynolds number airfoils. Lissaman's[3] seminal work in 1983 laid the foundation for understanding the efficiency of these airfoils, followed by H. Hu and Z Yang's[6] analysis of laminar flow separation, it was revealed that subtle differences in flow behavior depend on the Reynolds number. Experimental investigations by Selig et al.[7] produced pivotal data, driving forward the design considerations for low-Reynoldsnumber airfoils. Similarly, studies such as those by Sunada et al[8]. have demonstrated the significant disparities in characteristics between high and low Reynolds numbers.

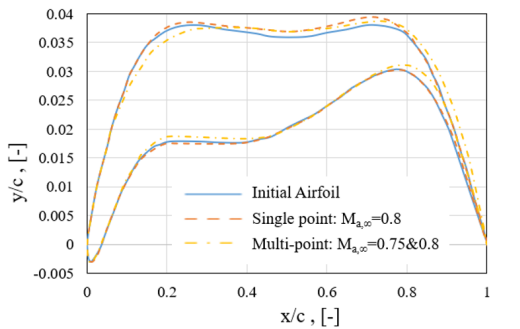
In 2020, Xu et al.[9] investigated the effect of Mach number on the flow around airfoil under subsonic and low Reynolds number conditions. The study may focus on the complex effects of flow field changes on performance near sound speed, including shock wave formation and flow separation. At high Mach numbers, when the velocity of the fluid flowing through the airfoil surface increases to be equal to the local sound velocity, a sonic line is formed and the flow field around the airfoil is divided into two distinct flow regions: subsonic region and supersonic region. In the supersonic region, the flow velocity of the fluid is higher than the local sound velocity, and the interaction and information transfer between fluid particles are no longer dependent on the pressure wave. Because the pressure change cannot propagate to the entire flow field in time, shock waves and shear layers appear in the supersonic region, which reduces the fluid velocity, significantly increases the pressure, and thickens the boundary layer. At the same time, a strong inverse pressure gradient region is formed on the airfoil surface, which makes the fluid in the boundary layer subject to greater resistance. The fluid flow rate decreases and the adhesion is weakened, which ultimately makes the fluid unable to continue to flow along the airfoil surface, resulting in vortex and turbulence and forming obvious separation phenomenon, and the resistance increases[10-12].

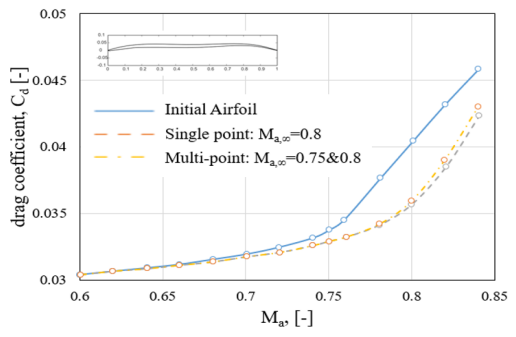
In this paper, experiments and simulations have been conducted on a rotor system specifically designed for flight in the Martian atmospheric environment. After verifying the agreement between CFD results and experimental data in the low-pressure and -density environment, the rotor was then scaled and numerical calculations were conducted in a simulated Martian environment. The thrust efficiency and flow characteristics of different rotor systems under various air densities and tip Mach numbers were elucidated. Finally, rotors were scaled for Mars environment and numerical computations were implemented to investigate the effects of different tip Mach numbers on the aerodynamic characteristics and flow field.

2. Numerical approaches

2.1 Arifoil selection for Mars applications

The low Reynolds number-transonic combination is unique in aeronautical applications and is unfortunately distinguished by a complete lack of suitable airfoil data. In previous studies [24], the effects of Mach number and angles of attack on aerodynamic characteristics of the optimized airfoils, NACA and Ultra-Thin airfoils, are investigated under low Reynolds number (Re = 17,000) and high-subsonic-flow ($M_{a,\infty}=0.6-0.9$) conditions. Figure 2 (a) shows the resulting optimized Ultra-Thin airfoil. The results indicate that the conventional airfoil exhibits a nearly parallel shift in the drag divergence Mach number curves across the entire range of Mach numbers. In contrast, the Ultra-Thin airfoil demonstrates a significant reduction in drag when subjected to Mach numbers greater than 0.75.





(a) Aorfoil geometries

(b) Drag divergence mach number

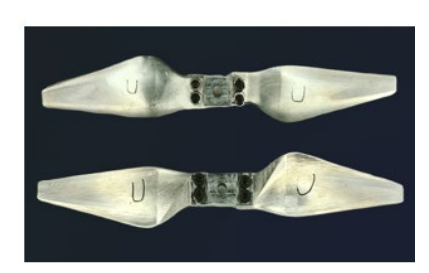
Figure 2 Initial airfoil and single-/multi-point optimized airfoils at Ma∞ =0.75 and 0.8^[4]

2.2 Rotor Design

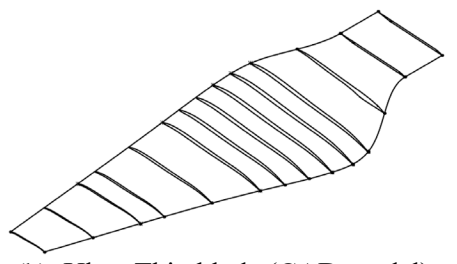
The primary objective of the propeller is to maximize the performance at its hovering stage, i.e., higher the figure of merit. Propellers operating at Mars condition face several unique design challenges that need to be addressed, including low dynamic pressure on the blades due to reduced air density and limited tip speed for minimizing compressibility losses. The Mars atmospheric conditions were assumed in this context correspond to the previous research work[13-15]. The key characteristics of the Mars atmosphere, in which the propeller will undergo computational simulation and experimental testing, are presented in Table 1. The impact of low-density environments on blade aerodynamic performance on Mars was investigated using three distinct density values, designated as MC1, MC2, and MC3 respectively. Furthermore, a comprehensive evaluation of the blade's aerodynamic performance was conducted through numerical simulation and experimental testing, specifically focusing on condition MC4 as outlined in Table 1.

The blade geometry is depicted in Figure 3, with the propeller diameter limited to 0.3m due to the maximum diameter of the testing chamber being 0.8m. The distribution of the blade chord length is designed to ensure a consistent Reynolds number, approximately 17,000, is maintained over a radial range of 40-80% on the blade in Figure 3 (g). This design consideration takes into account the specific characteristics of low Reynolds number - compressibility aerodynamics. It has been suggested by several experts that at low Reynolds numbers (Re = 10,000), compressibility introduces unique flow features such as elongated wakes[5] and vorticity-induced nonlinear lift[16] due to Kelvin-Helmholtz (KH) instability.

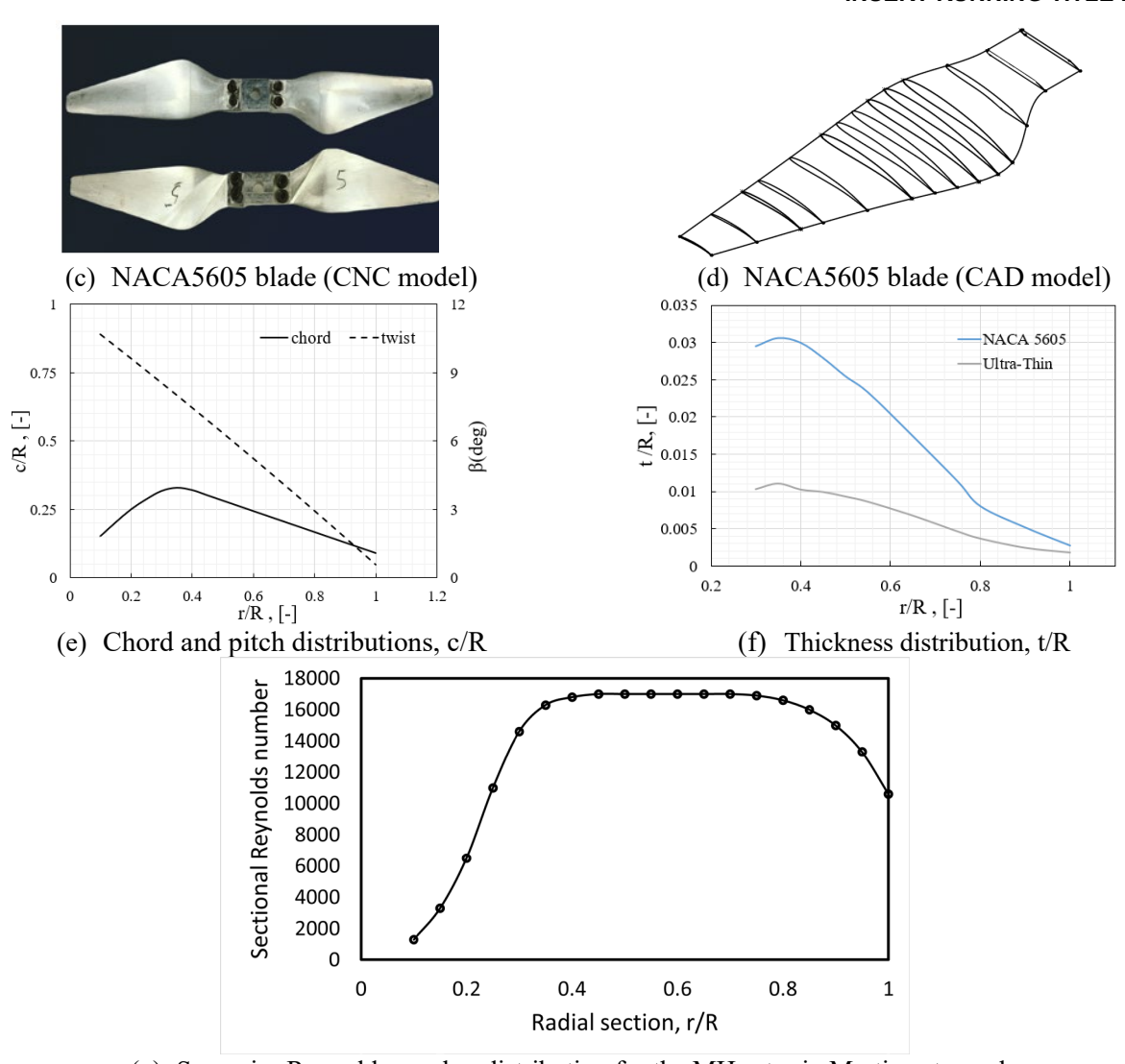
The rotor's spanwise pitch distribution, in Figure 3 (e), shows a linear distribution. However, appropriate pitch distribution can ensure the efficient performance of the rotor. By accurately adjusting the pitch distribution of the blade, the lift distribution of the rotor can be optimized under different flight conditions (such as hover, forward flight, side flight, etc.) [17]. Reduce vibration, reduce noise, and improve flight stability and economy.



(a) Ultra-Thin blade (CNC model)



(b) Ultra-Thin blade (CAD model)



(g) Sapnwise Reynolds number distribution for the MH rotor in Martine atmosphere

Figure 3 The design and specifications of the rotor blade's geometry

2.3 Rotor Simulation

The finite volume method is employed to numerically solve the three-dimensional unsteady Navier-Stokes equations, with consideration given to compressible and incompressible formulations for blade tip Mach numbers above and below 0.2, respectively. The operating conditions for the current study on rotor blade aerodynamic performance are presented in Table 1, encompassing the anticipated variations in atmospheric pressure, temperature, and density on Mars due to diurnal cycles[13]. The purpose of rotor numerical simulations is to conduct a more comprehensive comparison and validation with experimental data, thereby facilitating the optimization of rotor aerodynamic performance. The specific tasks can be divided into the following three parts:

The initial step involves conducting a comprehensive examination of the APC 9*6E propeller, encompassing the validation process that compares experimental findings with numerical calculations. Further elaboration can be found in Section 4.

Secondly, the aerodynamic performance of the single rotor system, NACA5605 and Ultra-thin CNCed blades, with a diameter of 0.217m in Figure 3 (a and c), was investigated through experimental and numerical analyses. Additionally, the experimental and simulation calculations were performed under specific operating conditions as outlined in Table 2, referred to as MC4. The experiments were conducted at a blade pitch angle of 8° for both NACA and Ultra-thin rotors, while the numerical simulations were carried out at several pitch angles, see Section 5.1.

After conducting a comparative analysis of the aerodynamic performance between NACA and Ultra-Thin rotors, the Ultra-Thin rotor has been selected for investigating its aerodynamic performance in the Martian environment. Initially, the model is scaled to meet the specific requirements of Mars, with a diameter of 1.2m. Additionally, an investigation is carried out on a single rotor at various Mach

numbers (0.6, 0.7, 0.75, 0.8, and 0.85) and blade pitch angles to obtain off-design aerodynamic performances, as show in Section 5.2. Finally, based on the results obtained from analyzing the aerodynamic performance of a single rotor under the aforementioned different conditions, further research is conducted to investigate the aerodynamic performance of a coaxial rotor, in Section 5.3, with tip Mach numbers of 0.75 and 0.85, a pitch angle of 12 degrees, while maintaining a rotor spacing apart distance equal to h/D = 0.1.

Variable	Numerical (Mars)			Exp/Num (Earth)
	MC1	MC2	MC3	MC4
Density [kg/m³]	0.02	0.0175	0.012	0.14
Heat capacity ratio [-]	1.289	1.289	1.289	1.4
Dynamic viscosity [kg/(m·s)]	1.289×10 ⁻⁵	1.289×10 ⁻⁵	1.289×10 ⁻⁵	1.73×10 ⁻⁵
Temperature [K]	210	223	285	304
Pressure [Pa]	793	738	640	12350

Table 1 Different operating conditions for evaluating rotor performance

3. Experimental Methodology

3.1 Test setup

The experiments were conducted at the low-density and -pressure chamber (LDPC) situated in the National Key Laboratory of Helicopter Aeromechanics at NanJing University of Aeronautics and Astronautics, as shown in Figure 4. The LDPC system comprised four primary independent components: a circular evacuation chamber, a three-component force balance system designed for measuring propeller forces and moments in three directions, a propeller mounting structure, and a data-acquisition system as illustrated in Figure 4.

The evacuation chamber has a diameter of 0.8 meters and a length of 2 meters, while employing a root pump system to achieve the desired working pressure level. The pump system is equipped with a digital pressure level display. The total pressure level is regulated by adjusting the butterfly valve situated within the flexible pipe.

The three-component force balance system, in Figure 4, incorporates a highly precise load cell with a diameter of 36mm and a height of 20mm. It boasts an accuracy level of ±0.03% F.S., The range of load cells for thrust and torque measurements is 50 N and 2 Nm, respectively. During the data acquisition, the sensor is capable of collecting 1000 data points per second and automatically storing them in Excel spreadsheets. The utilized speed measuring instrument is a laser velocimeter with a speed range of 1~99999 revolution per minuite, a resolution of 0.01RPM, and an accuracy of ±0.02%.

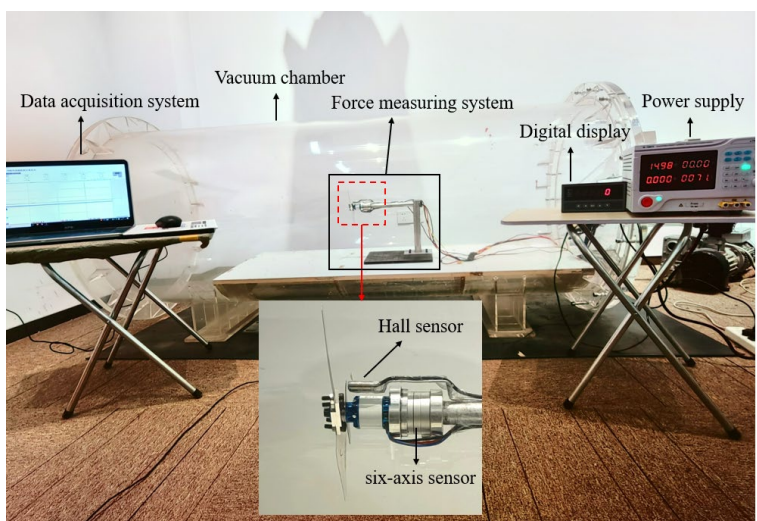


Figure 4 Low-pressure and -density experimental testing system.

3.2 Experimental data and post-processing

During each rotor test, the variables, forces and moments, are measured twice with a sampling time ranging from 80 to 150 seconds. For variables that can be expressed as linear functions of directly measured independent variables, the mean value and standard deviation can be calculated based on the measured values. All experimental results will have a confidence level of 95%. The sampled data is averaged using Eq. 1 following the method proposed by Hughes and Hase in $2010^{[18]}$, aiming to enhance the achieved accuracy. A widely accepted quantitative measure of dispersion is the sample standard deviation, denoted as Δx . In the case where all data points have equal weight, the sample standard deviation can be defined by the

Eq. 2. Hence, the average value error was computed using Eq. 3.

$$\bar{x} = \frac{\sum_{i}^{m} x_{i}}{m}$$
Eq. 1
$$s = \sqrt{\frac{\sum (x_{i} - \bar{x})^{2}}{m - 1}}$$

$$\Delta \bar{x} = \frac{s}{\sqrt{m}}$$
Eq. 2

where x_i is the measured value, \bar{x} is the averaged value, and m is the number of measured values. Taking the measured values at a rotational speed of 6730 RPM, when the number of points is unified to 500, the distribution curve of the thrust with the speed obtained by the three data processing methods is shown in Figure 5

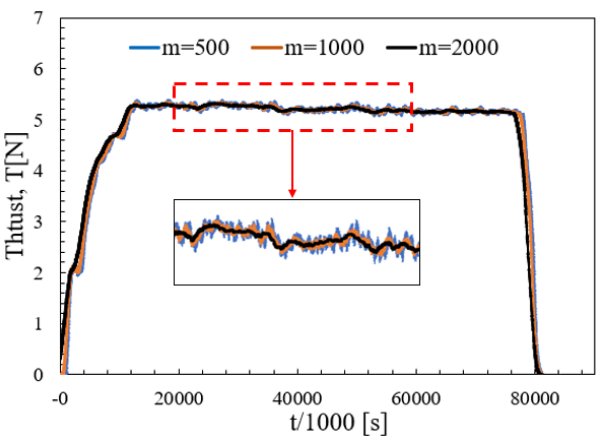


Figure 5 data post-processing

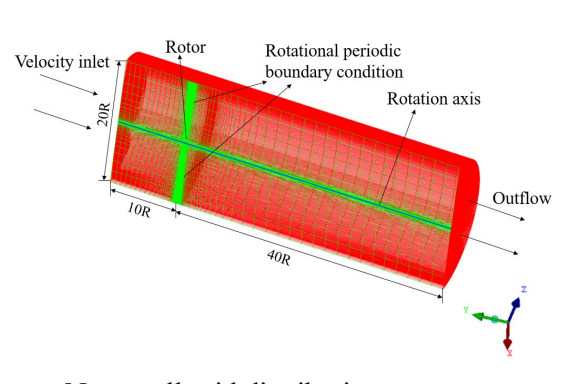
4. Validation Case

Due to the small thrusts exerted by these propellers, it is necessary to employ sensitive equipment that can minimize experimental uncertainties and ensure reliable results. The selection of APC 11x8E propellers was based on the availability of performance data from the University of Illinois at Urbana-Champaign (UIUC)^[19], as shown in Figure 6. In this section, we have precisely studied APC propeller experimentally and numerically.

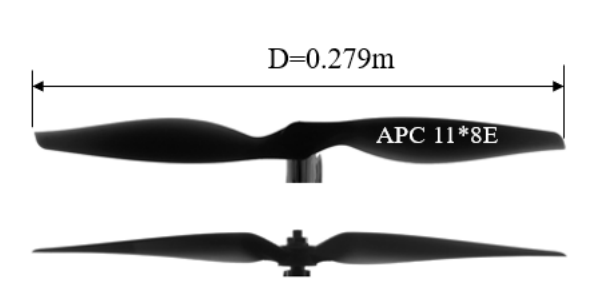
The numerical approach was demonstrated through a validation case, where the current computational results were compared to the previous experimental results of the APC propeller^[20]. A structured mesh, featuring an O-grid mesh topology, was employed around the propeller to accurately capture the intricate flow field in proximity to the boundary layer, as shown in Figure 6 (b). For the MRF method, a periodic boundary condition is implemented at the blade root plane, as illustrated in Figure 6 (a). The no-slip wall boundary condition is enforced on the surface of the blade. In order to minimize the influence of farfield boundary conditions, a computational domain with an upstream distance of 10 R, a downstream distance of 40 R, and an outer boundary radius of 10 R from the rotating axis.

The experiment measured the thrust of the selected propeller at a rotation speed ranging from 3000RPM to 7000RPM under hover/static conditions. The thrust coefficients at the static conditions exhibit consistency between UIUC's experimental results and our own, including both numerical and

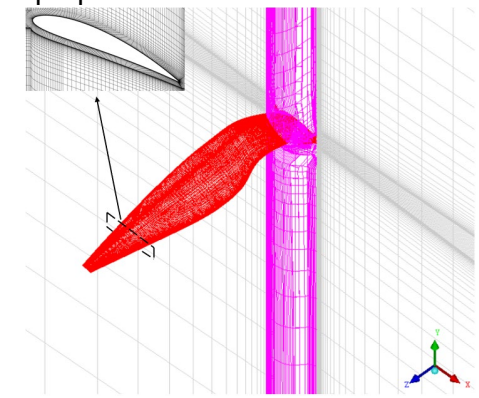
experimental data, as depicted in Figure 6 (d) for the APC propellers.



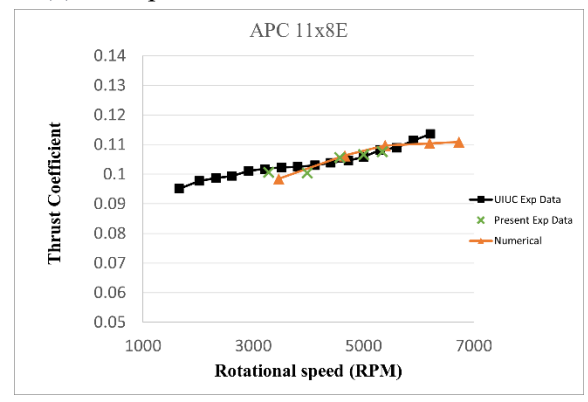
(a) Near-wall grid distribution



(c) The side and front view of APC propeller



(b) Computational domain



(d) Static performance of APC propellers at different speeds

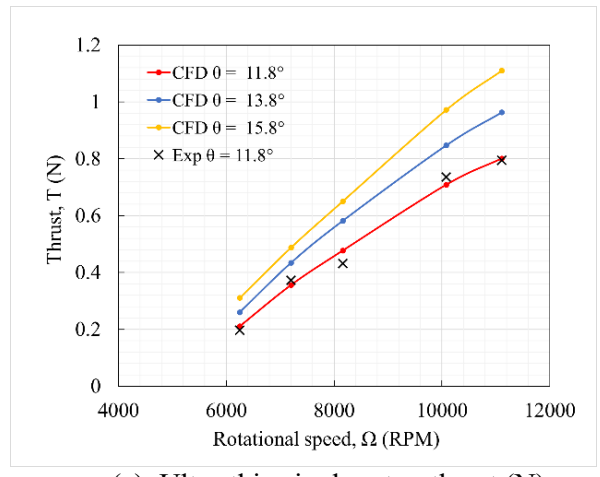
11*8E

Figure 6 Numerical and experimental analysis of the APC 11*8E propeller

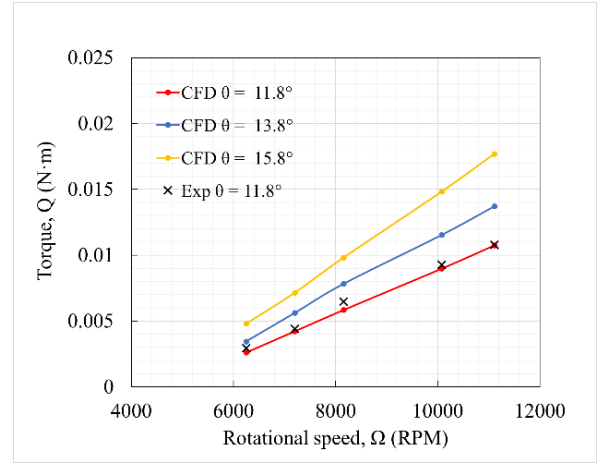
5. Results and Discussion

5.1 Single-rotor Performance Predictions under the MC4 condition

Figure 7 shows the comparison between the experimental and simulated results under MC4 condition, as shown in Table 1. The experimental results of the rotor's thrust and torque at pitch angle of are in excellent agreement with the simulation results within the measured speed range, thereby affirming the reliability of the CFD calculation employed in this study. Figure 7(a) shows the variation of the generated thrust T with the rotational speed of the tested rotor. The increase in the pitch angle of the test rotor is observed to result in an augmentation of both generated thrust and torque. The same trend on thrust curve was also observed through experiments conducted by the University of Maryland^[21] and Harbin Institute of Technology^[22].



(a) Ultra-thin single rotor, thrust (N)



(b) Ultra-thin single rotor, torque (N·m)

Figure 7 Single rotor performance under MC4 operating condition: Ultra-thin blade

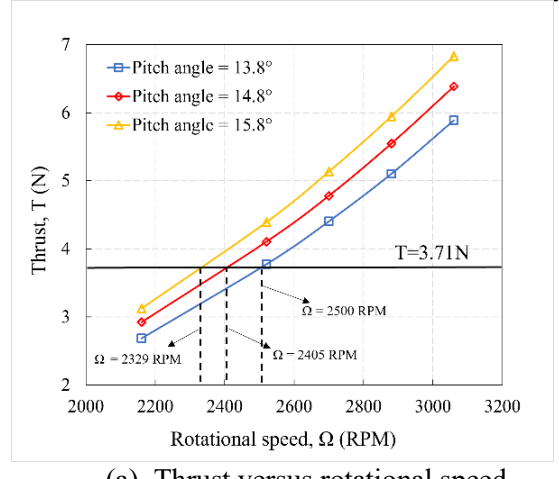
5.2 Single-rotor Performance Predictions under the Martian Atmosphere condition

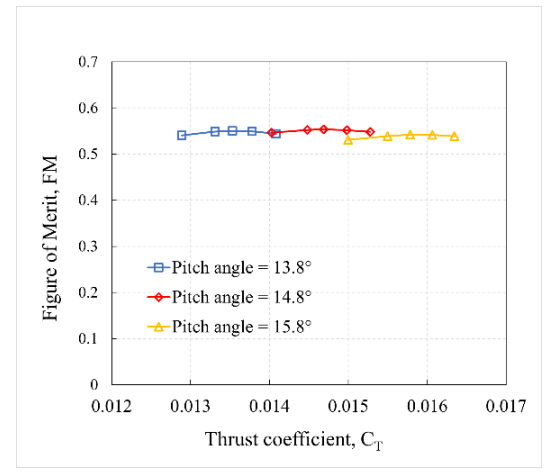
The UT single rotor was chosen for the investigation of aerodynamic performance in the Martian environment. The UT rotor is therefore scale-up to match the dimensions of the "ingenuity" [13], specifically referring to the rotor diameter, i.e. D = 1.21m. The design of the Mars helicopter features a co-axial rotor with a mass of roughly 2.0 kg, resulting in an equivalent force of about 7.42N under the gravitational condition on Mars. Therefore, the thrust generated by each rotor of a coaxial rotor system must be no less than 3.71N, i.e. Treq = 3.71 N per rotor.

The significance of the Mach number was found to be less pronounced in experimental studies when the Mach number falls below 0.6, as pointed out by Anyoji et al. [23] However, when the Mach number exceeds 0.6, the findings indicate that compressibility tends to elongate the airfoil's wake and hinder early roll-up of the shear layer on the upper surface [4, 5]. The investigation of compressibility effects, under the condition MC1 in Table 1, is therefore conducted to enhance the understanding of the overall performance of the UT rotor in the Martian environment. Computations are performed for a series of pitch angles of the rotor $\phi = 13.8^{\circ}$, 14.8° , and 15.8° , for blade tip Mach numbers 0.6, 0.7, 0.75, 0.8 and 0.85, with a corresponding chord Reynolds number of 18670, 21781, 24893, and 26449 at 75% of the rotor radius.

Figure 8 shows the calculated hovering performance of the UT single rotor at various collective pitch angles under the Martian atmosphere. The effect of collective pitch angle on the hovering performance of the UT rotor is characterized by an upward shift in the performance curve, as shown in Figure 8 (a). In addition, the UT single rotor system is capable of achieving a hovering state on Mars when its rotational speed reaches 2329 RPM, resulting in a thrust force of 3.71N (equivalent to 1kg per rotor). In contrast, the Harbin Institute of Technology's design requires a rotational speed of 4000 RPM to obtain a thrust force of 1.855N (equivalent to 0.5 kg) for their hovering condition^[22], while the 'ingenuity' can generate a maximum thrust force of 6.625N per rotor at 2600 RPM^[13].

The figure of merit is defined as the ratio of the ideal induced power to the actual power of the rotor. However, accurately calculating the induced power caused by the wake presents challenges in determining this value. A well-designed rotor typically achieves a figure of merit (FM) ranging from 0.7 to 0.8 at earth atomsphere condition^[24]. Figure 8 (b) shows the FM versus thrust coefficient for UT single rotor models calculated for MC1 conditions. The numerical results demonstrate that the figure of merit of the UT single rotor system remains consistently around 0.55 for all three collective pitch angles, even as the rotational speed increases. In contrast, the optimal FM value that 'Ingenuity', i.e., the coaxial rotor, can achieve is approximately 0.62.





(a) Thrust versus rotational speed (b) Thrust coefficient versus FM Figure 8 Hovering performance of Ultra-thin single rotor for $\rho = 0.02 \, kg/m^3$.

Figure 9 and Figure 10 show the average pressure coefficient (C_P) distribution of the upper and lower surfaces of the Ultra-Thin blade at 13.8 ° and 15.8 ° pitch angles, respectively. The expansion of the negative pressure zone along the chordwise direction towards the trailing edge near the blade tip is observed in Figure 9 as the tip Mach number increases from 0.6 to 0.85, while there is no significant alteration in the radial direction towards the blade root. However, it is worth mentioning that the increase in the blade pitch angle from 13.8 to 15.8 degrees leads to an expansion of the negative pressure zone at the blade tip location, both in terms of spanwise and radial directions, as shown in Figure 10.

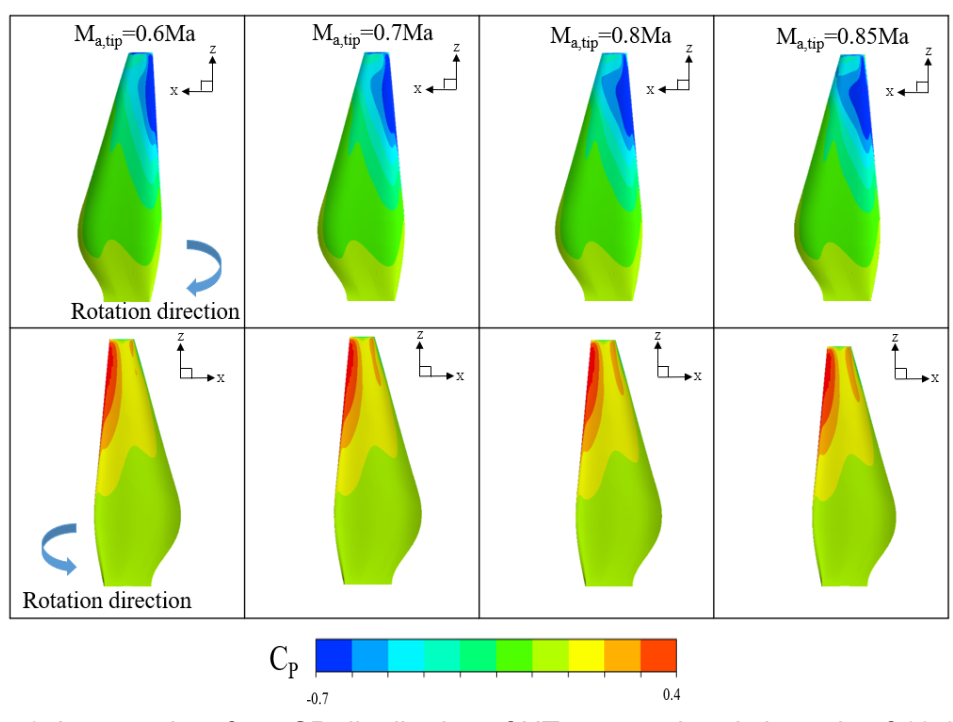


Figure 9 Averaged surface CP distribution of UT rotor at the pitch angle of 13.8 deg.

(Upper: Blade upper surface, Lower: Blade lower surface).

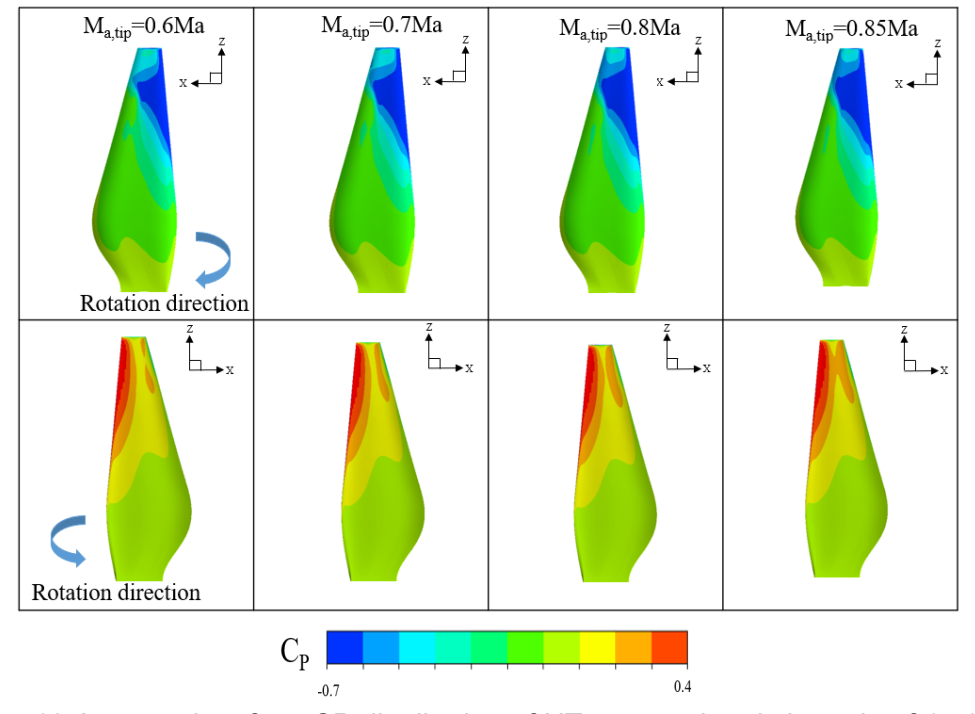


Figure 10 Averaged surface CP distribution of UT rotor to the pitch angle of 15.8 deg.

(Upper: Blade upper surface, Lower: Blade lower surface).

Figure 12 shows the pressure contour and streamlines around the airfoil at the radial location r/R = 0.90 at the pitch angle of 13.8°. The analysis was conducted to investigate the influence of Mach number effects on the flow past though radial stations for the rotor blade, revealing a significant impact on flow separation and subsequent wake patterns. The results indicated that compressibility has a tendency to elongate the wake of the airfoil, shown in Figure 12, and hinder the early roll-up of the upper shear layer, which is consistent with previous observations made by Desert et al. [5]. The pressure coefficient distributions along the chordwise at radial station r/R of 0.9 are depicted in Figure 11. The occurrence of a pressure suction spike followed by a flat plateau is observed when the Mach

INSERT RUNNING TITLE HERE

number is less than or equal to 0.7, which is attributed to the leading-edge separation bubble. As the Mach number increases to 0.75 and 0.8, a weak shock is formed on the nose of the airfoil, and the shock-separation interaction is observed, as sahown in Figure 13.

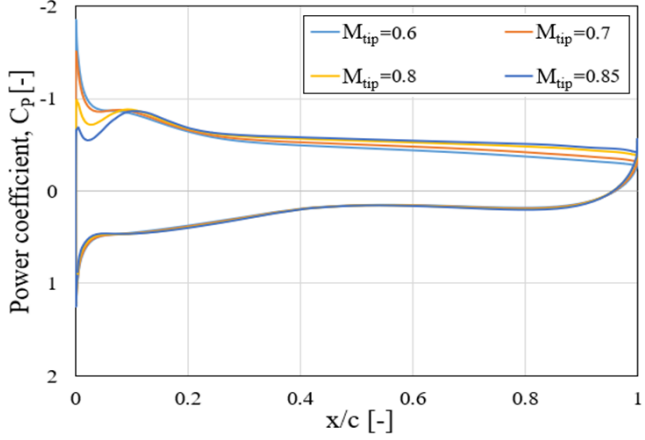


Figure 11 Averaged surface CP distribution at the cross section of the rotor r/R = 0.90 to the pitch angle of 13.8 deg.

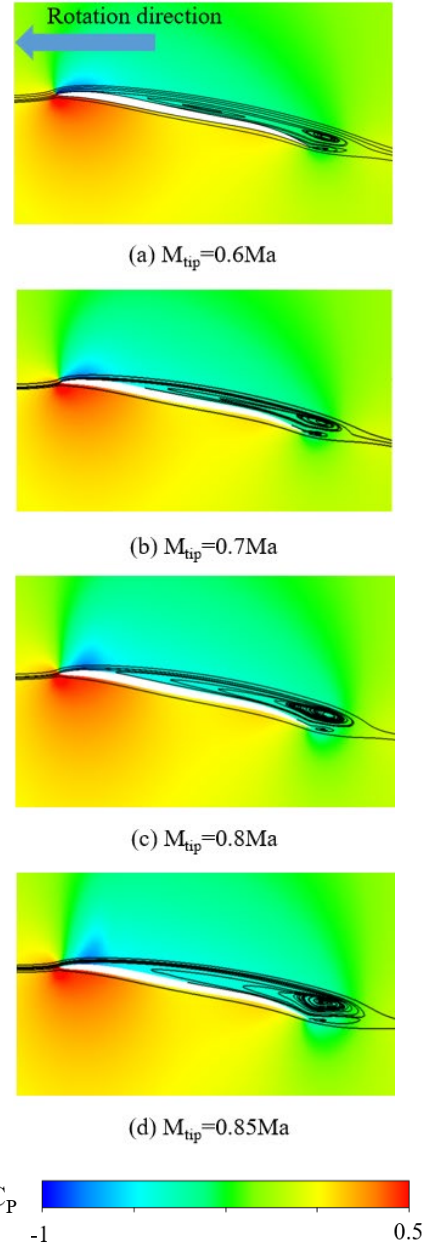


Figure 12 Averaged CP and streamline distributions at the location r/R=0.90 to the pitch angle of 13.8deg.

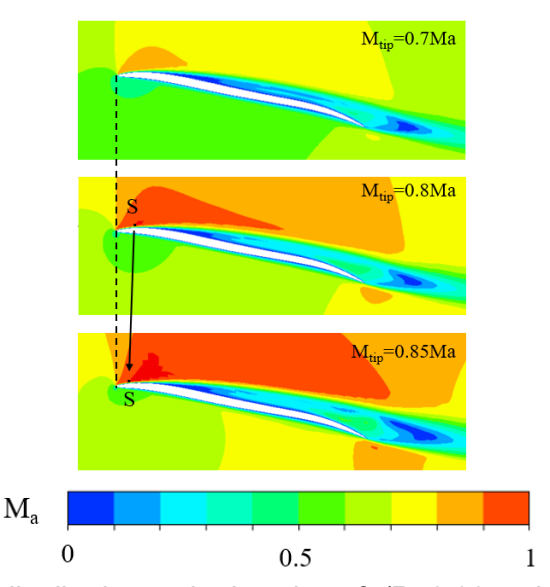


Figure 13 Mach number distribution at the location of r/R=0.90 to the pitch angle of 13.8deg

6. Conclusion and Future Work

The present study has focused on conducting experimental and numerical investigations into the performance of a Mars helicopter rotor, which operates at a Reynolds number of 17,000 at 75% radial location and within a relatively higher Mach number range of 0.6–0.85. The subsequent conclusions drawn from this research are as follows.

- (1) A comprehensive examination of the APC propeller is conducted, and it is observed that the thrust coefficients and FM at static conditions exhibit consistency between UIUC's experimental results and our own findings, with a noticeable difference falling within a range of 3%. However, on the numerical side, the thrust and FM values obtained using the CFD MRF method at various mesh densities for the APC 9*6E propeller, encompassing rotational speeds ranging from 3460 to 6730 RPM. The FM results exhibit excellent agreement with experimental data at moderate rotational speeds, while marginally underestimating values at low and high rotational speeds.
- (2) The aerodynamic performance of the single rotor system equipped with Ultra-thin CNCed blades, featuring a diameter of 0.217m, was investigated through both experimental and numerical analyses. The experimental results of both rotor's thrust and torque at pitch angle of are in excellent agreement with the simulation results within the measured speed range. Additionally, the Ultra-thin rotor exhibits a highe maximum FM value of 0.69 at a pitch angle of 13.8°, with a rotational speed of 7200 RPM.
- (3) The aerodynamic performance of the Ultra-thin rotor in the Martian environment demonstrates that the influence of collective pitch angle on the hovering capability of the UT rotor is characterized by an upward shift in the performance curve. Specifically, when its rotational speed reaches 2329 RPM, the UT single rotor system can achieve a hovering state on Mars, resulting in a thrust force of 3.71N (equivalent to 1kg per rotor). On the other hand, the expansion of the blade tip negative pressure zone along the chordwise direction towards the trailing edge is observed as the blade tip Mach number increases from 0.6 to 0.85. However, an increase in the blade pitch angle from 13.8 to 15.8 degrees results in an expansion of the blade tip negative pressure zone in both spanwise and radial directions.

The future study will involve parametrically evaluating various rotor design parameters, including blade airfoil, planform shape, twist, and rotor solidity under Martian air density conditions. The objective is to systematically enhance aerodynamic performance in order to increase efficiency. These experiments will also encompass a range of Reynolds and Mach numbers, which will be instrumental in the development of rotors at different scales.

7. Contact Author Email Address

Corresponding author: Zhaolin Chen, and email: <u>zhaolin_chen@nuaa.edu.cn</u>

8. Copyright Statement

The authors confirm that they, and/or their company or organization, hold copyright on all of the original material included in this paper. The authors also confirm that they have obtained permission, from the copyright holder of any third party material included in this paper, to publish it as part of their paper. The authors confirm that they give permission, or have obtained permission from the copyright holder of this paper, for the publication and distribution of this paper as part of the ICAS proceedings or as individual off-prints from the proceedings.

9. Funding

The author(s) disclosed receipt of the following financial support for the research, authorship, and/or publication of this article: The present work is supported by the National Natural Science Foundation of China under Grant No. 12002161, 12032011, and the National Key Laboratory of Helicopter Aeromechanics, Funding No. 2023-HA-LB-067-06.

References

- [1] Rafkin, S. C. R., and Banfield, D. "On the problem of a variable Mars atmospheric composition in the determination of temperature and density from the adiabatic speed of sound," *Planetary and Space Science*, Vol. 193, 2020, p. 105064
- [2] Pla-García, J., Rafkin, S. C. R., Martinez, G. M., Vicente-Retortillo, Á., Newman, C. E., Savijärvi, H., de la Torre, M., Rodriguez-Manfredi, J. A., Gómez, F., Molina, A., Viúdez-Moreiras, D., and Harri, A.-M. "Meteorological Predictions for Mars 2020 Perseverance Rover Landing Site at Jezero Crater," *Space Science Reviews*, Vol. 216, No. 8, 2020, p. 148
- [3] Lissaman, P. B. S. "Low Reynolds Number Airfoils" *Journal of Fluid Mechanics*, Vol. 15, 1983, pp. 223-239
- [4] Chen, Z., Wei, X., Xiao, T., and Qin, N. "Optimization of transonic low-Reynolds number airfoil based on genetic algorithm," *Proceedings of the Institution of Mechanical Engineers, Part G: Journal of Aerospace Engineering,* Vol. 238, No. 1, 2023, pp. 44-60
- [5] Désert, T., Jardin, T., Bézard, H., and Moschetta, J. M. "Numerical predictions of low Reynolds number compressible aerodynamics," *Aerospace Science and Technology*, Vol. 92, 2019, pp. 211-223
- [6] Yang, Z., and Hu, H. "Laminar Flow Separation and Transition on a Low-Reynolds-Number Airfoil," *Journal of aircraft,,* Vol. 45, No. 3, 2008, pp. 1067-1070
- [7] Selig, M., and McGranahan, B. "Wind Tunnel Aerodynamic Tests of Six Airfoils for Use on Small Wind Turbines," *42nd AIAA Aerospace Sciences Meeting and Exhibit*. American Institute of Aeronautics and Astronautics, 2004.
- [8] Sunada, S., Sakaguchi, A., and Kawachi, K. "Airfoil Section Characteristics at a Low Reynolds Number," *Journal of Fluids Engineering*, Vol. 119, No. 1, 1997, pp. 129-135
- [9] Xu, J.-H., Song, W.-P., Han, Z.-H., and Zhao, Z.-H. "Effect of mach number on high-subsonic and low-Reynolds-number flows around airfoils," Vol. 34, No. 14n16, 2020, p. 2040112
- [10] Smyrl, J. L. "The impact of a shock-wave on a thin two-dimensional aerofoil moving at supersonic speed," *Journal of Fluid Mechanics*, Vol. 15, No. 2, 1963, pp. 223-240
- [11] Zhao, Z., Ren, X., Gao, C., Xiong, J., Liu, F., and Luo, S. "Experimental Study of Shock Wave Oscillation on SC(2)-0714 Airfoil," *51st AIAA Aerospace Sciences Meeting including the New Horizons Forum and Aerospace Exposition*. American Institute of Aeronautics and Astronautics, 2013.
- [12] Börner, M., and Niehuis, R. "Dynamics of Shock Waves Interacting With Laminar Separated Transonic Turbine Flow Investigated by High-Speed Schlieren and Surface Hot-Film Sensors," *Journal of Turbomachinery*, Vol. 143, No. 5, 2021,
- [13] Koning, W. J. F., Johnson, W., and Grip, H. F. "Improved Mars Helicopter Aerodynamic Rotor Model for Comprehensive Analyses," Vol. 57, No. 9, 2019, pp. 3969-3979
- [14] Withrow-Maser, S., Johnson, W., Young, L., Koning, W., Kuang, W., Malpica, C., Balaram, J., and Tzanetos, T. "Mars Science Helicopter: Conceptual Design of the Next Generation of Mars Rotorcraft," *Accelerating Space Commerce, Exploration, and New Discocery Conference*. 2020.
- [15] Koning, W. J. F., Koning, W. J. F., and Koning, W. J. F. "ELISA: A Tool for Optimization of Rotor Hover Performance at Low Reynolds Number in the Mars Atmosphere." 2024.
- [16] Munday, P. M., Taira, K., Suwa, T., Numata, D., and Asai, K. "Nonlinear Lift on a Triangular

- Airfoil in Low-Reynolds-Number Compressible Flow," Vol. 52, No. 3, 2015, pp. 924-931
- [17] Tang, D. M., and Dowell, E. H. "Flutter and stall response of a helicopter blade with structural nonlinearity," Vol. 29, No. 5, 1992, pp. 953-960
- [18] Ifan G. Hughes, and Hase, T. P. A. *Measurements and their Uncertainties: A Practical Guide to Modern Error Analysis*: Oxford University Press, USA, 2010.
- [19] Deters, R. W., Ananda Krishnan, G. K., and Selig, M. S. "Reynolds Number Effects on the Performance of Small-Scale Propellers," *32nd AIAA Applied Aerodynamics Conference*. American Institute of Aeronautics and Astronautics, 2014.
- [20] Deters, R., Ananda, G., and Selig, M. "Slipstream Measurements of Small-Scale Propellers at Low Reynolds Numbers," *Aerospace Engineering*. Vol. Ph.D, University of Illinois at Urbana-Champaign, 2014.
- [21] Shrestha, R., Benedict, M., Hrishikeshavan, V., and Chopra, I. "Hover Performance of a Small-Scale Helicopter Rotor for Flying on Mars," *Journal of Aircraft*, Vol. Vol.53, No. No.4, 2016, pp. 1160-1167
- [22] Zhao, P., Quan, Q., Chen, S., Tang, D., and Deng, Z. "Experimental investigation on hover performance of a single-rotor system for Mars helicopter," *Aerospace Science and Technology*, Vol. 86, No. 0, 2019, pp. 582-591
- [23] Anyoji, M., Numata, D., Nagai, H., and Asai, K. "Effects of Mach Number and Specific Heat Ratio on Low-Reynolds-Number Airfoil Flows," Vol. 53, No. 6, 2015, pp. 1640-1654
- [24] Conlisk, A. T. "Modern helicopter rotor aerodynamics," *Progress in Aerospace Sciences,* Vol. 37, No. 5, 2001, pp. 419-476